Biogeosciences, 18, 1333–1350, 2021
https://doi.org/10.5194/bg-18-1333-2021

Biogeosciences Open Access EGU

Changing sources and processes sustaining surface CO_2 and CH_4 fluxes along a tropical river to reservoir system

Cynthia Soued and Yves T. Prairie

Groupe de Recherche Interuniversitaire en Limnologie et en Environnement Aquatique (GRIL), Département des Sciences Biologiques, Université du Québec à Montréal, Montréal, H2X 3X8, Canada

Correspondence: Cynthia Soued (cynthia.soued@gmail.com)

Received: 6 July 2020 – Discussion started: 14 September 2020
Revised: 15 January 2021 – Accepted: 18 January 2021 – Published: 22 February 2021

Abstract. Freshwaters are important emitters of carbon dioxide (CO_2) and methane (CH_4), two potent greenhouse gases (GHGs). While aquatic surface GHG fluxes have been extensively measured, there is much less information about their underlying sources. In lakes and reservoirs, surface GHG can originate from horizontal riverine flow, the hypolimnion, littoral sediments, and water column metabolism. These sources are generally studied separately, leading to a fragmented assessment of their relative role in sustaining CO_2 and CH_4 surface fluxes. In this study, we quantified sources and sinks of CO_2 and CH_4 in the epilimnion along a hydrological continuum in a permanently stratified tropical reservoir (Borneo). Results showed that horizontal inputs are an important source of both CO_2 and CH_4 ($> 90\,\%$ of surface emissions) in the upstream reservoir branches. However, this contribution fades along the hydrological continuum, becoming negligible in the main basin of the reservoir, where CO_2 and CH_4 are uncoupled and driven by different processes. In the main basin, vertical CO_2 inputs and sediment CH_4 inputs contributed to on average 60 % and 23 % respectively to the surface fluxes of the corresponding gas. Water column metabolism exhibited wide amplitude and range for both gases, making it a highly variable component, but with a large potential to influence surface GHG budgets in either direction. Overall our results show that sources sustaining surface CO_2 and CH_4 fluxes vary spatially and between the two gases, with internal metabolism acting as a fluctuating but key modulator. However, this study also highlights challenges and knowledge gaps related to estimating ecosystem-scale CO_2 and CH_4 metabolism, which hinder aquatic GHG flux predictions.

1 Introduction

Surface inland waters are globally significant sources of greenhouse gases (GHGs) to the atmosphere, namely carbon dioxide (CO_2) and methane (CH_4) (Bastviken et al., 2011; DelSontro et al., 2018a; Raymond et al., 2013). Freshwaters act as both transport vessels for terrestrial carbon (C) and as active biogeochemical processors, making them key sites of GHG exchange with the atmosphere (Tranvik et al., 2018). The impoundment of rivers for hydropower generation, irrigation, flood control, or other purposes changes the landscape and its C cycling (Maavara et al., 2017), often resulting in increased aquatic CO_2 and CH_4 emissions due to the decay of flooded organic matter (Prairie et al., 2018; Venkiteswaran et al., 2013). Globally, reservoirs are estimated to emit between 0.5 and 2.3 $PgCO_2eq\,yr^{-1}$ (Barros et al., 2011; Bastviken et al., 2011; Deemer et al., 2016; St. Louis et al., 2000), and this number is predicted to increase with a rapid growth of the hydroelectric sector in the upcoming decades (Zarfl et al., 2015). Several studies have focused on quantifying GHG surface diffusion from reservoirs around the world and have found extremely high variability temporally and spatially (Barros et al., 2011; Deemer et al., 2016), as is found in natural lakes (DelSontro et al., 2018a; Raymond et al., 2013). However, less research exists on the relative contribution of the different sources and processes sustaining surface diffusive fluxes and their variability in reservoirs.

GHG sources to surface waters can be both internal and external. The magnitude of allochthonous inputs, namely terrestrial organic and inorganic C, is known to increase with soil–water connectivity (Hotchkiss et al., 2015) and with soil C content and leaching capacity (Kindler et al., 2011; Li

et al., 2017; Monteith et al., 2007). Soil-derived gas inputs are also temporally variable, generally increasing with discharge, like during storm events (Vachon and del Giorgio, 2014) or rainy seasons (Kim et al., 2000; Zhang et al., 2019). Terrestrial inputs in the form of organic C can indirectly sustain surface GHG emissions by fuelling lake and reservoir in situ organic matter respiration (Karlsson et al., 2007; Pace and Prairie, 2005; Rasilo et al., 2017).

The net internal balance between production and consumption processes of CO_2 and CH_4 ultimately determines their surface fluxes. For CO_2, aerobic ecosystem respiration (ER) and gross primary production (GPP) are highly variable in space and time and generally a function of temperature, organic C content, and nutrients (Hanson et al., 2003; Pace and Prairie, 2005; Prairie et al., 1989; Solomon et al., 2013). Net heterotrophy (ER > GPP) is mainly associated with systems receiving high external inputs of organic C (Bogard et al., 2020; Tank et al., 2010; Wilkinson et al., 2016), while net autotrophy (ER < GPP) has been associated with highly productive nutrient-rich systems (Hanson et al., 2003; Sand-Jensen and Staehr, 2009). However, a large part of the variability in measured metabolic rates remains unexplained (Bogard et al., 2020; Coloso et al., 2011; Solomon et al., 2013), impeding our ability to accurately predict their net balance. Additionally, anaerobic C transformation adds another level of complexity to the C metabolic balance by decoupling GPP and ER (Bogard and del Giorgio, 2016; Martinsen et al., 2020; Vachon et al., 2020). For instance, acetoclastic methanogenesis can transform organic C to CH_4 instead of CO_2, and hydrogenotrophic methanogenesis converts CO_2 to CH_4 without producing O_2.

For CH_4, production occurs in both profundal and littoral sediments, and CH_4 reaches the water surface by vertical or lateral diffusive processes (Bastviken et al., 2008; DelSontro et al., 2018b; Encinas Fernández et al., 2014; Guérin et al., 2016). However, there is increasing evidence that CH_4 production in the oxic water column can also contribute significantly to lake CH_4 emissions (Bižić et al., 2019; Bogard et al., 2014; DelSontro et al., 2018b; Donis et al., 2017; Tang et al., 2014). Methanogenesis can be counter-balanced by the oxidation of CH_4 to CO_2 mainly in oxic and hypoxic environments (Conrad, 2009; Reis et al., 2020; Thottathil et al., 2019). While several studies have measured rates of CH_4 production and oxidation in lakes and reservoirs, few have quantified the net balance of these two processes at an ecosystem scale (Bastviken et al., 2008; Schmid et al., 2007), a balance tightly linked to physical processes within the water column (Vachon et al., 2019).

For both gases, physical mixing in lakes and reservoirs indirectly impacts C metabolic processes by shaping the O_2 profile and directly affects GHG surface diffusion by controlling the transport of CO_2 and CH_4 from deep to surface water layers (Barrette and Laprise, 2005; Kreling et al., 2014; Pu et al., 2020). Despite its potential importance (Kankaala et al., 2013), very few studies quantified vertical gas transport and the role of this process in fuelling surface GHG emissions. The movement of gases within a system depends on the structure of the water column, which changes spatially along the aquatic continuum. Reservoirs in particular exhibit strong gradients in morphometry and hydrology, translating into high spatial heterogeneity in surface GHG fluxes to the atmosphere (Paranaíba et al., 2018; Teodoru et al., 2011).

Understanding what regulates surface CO_2 and CH_4 concentrations and fluxes to the atmosphere thus requires knowledge of the interplay between all physical and biogeochemical processes involved and how they vary spatially. While a number of studies have assessed some processes individually or by difference, very few have measured all relevant components of the epilimnetic mass balance simultaneously. Here we report on a field study in a tropical East Asian hydropower reservoir quantifying external inputs, sediment inputs, net CO_2 and CH_4 metabolism, vertical diffusion from deeper layers, and gas exchange at the air–water interface. This allowed us to estimate the relative contribution of each process in shaping surface GHG emissions from the reservoir and to test whether the epilimnetic mass balance can be closed. The two major rivers feeding the reservoir flow into two elongated branches, acting as transition zones, before reaching the main basin. This configuration, common in reservoirs, allowed us to quantify and compare epilimnetic CO_2 and CH_4 regulation in two morphometrically different areas (reservoir branches and main basin). Overall, the aim of this study is to provide an ecosystem-scale portrait of the processes sustaining surface CO_2 and CH_4 emissions and examine how they change when transitioning from a river delta to an open basin.

2 Materials and methods

2.1 Site and sampling description

The study was conducted in the Batang Ai hydroelectric reservoir in Sarawak, Malaysia (latitude 1.16° and longitude 111.9°). The reservoir is located in Borneo in a tropical equatorial climate with a constantly high temperature averaging 23 and 32 °C during nighttime and daytime respectively (Sarawak Government, 2019). The region experiences two weak monsoon seasons (November to February and June to October) with a yearly average rainfall of 3300 to 4600 mm (Sarawak Government, 2019). The reservoir was impounded in 1985 with a dam wall of 85 m, a surface area of $\sim 68.4\,km^2$, and a watershed area of $1149\,km^2$ of mostly undisturbed forested land (limited rural habitations and small-scale croplands).

We distinguish between three sections of the study site: inflows, reservoir branches, and the reservoir main basin shown in Fig. 1. The inflows are the two main reservoir inlets: the Batang Ai and Engkari rivers (3 to 10 m deep where sampled). The two rivers flow into two arms that we refer to

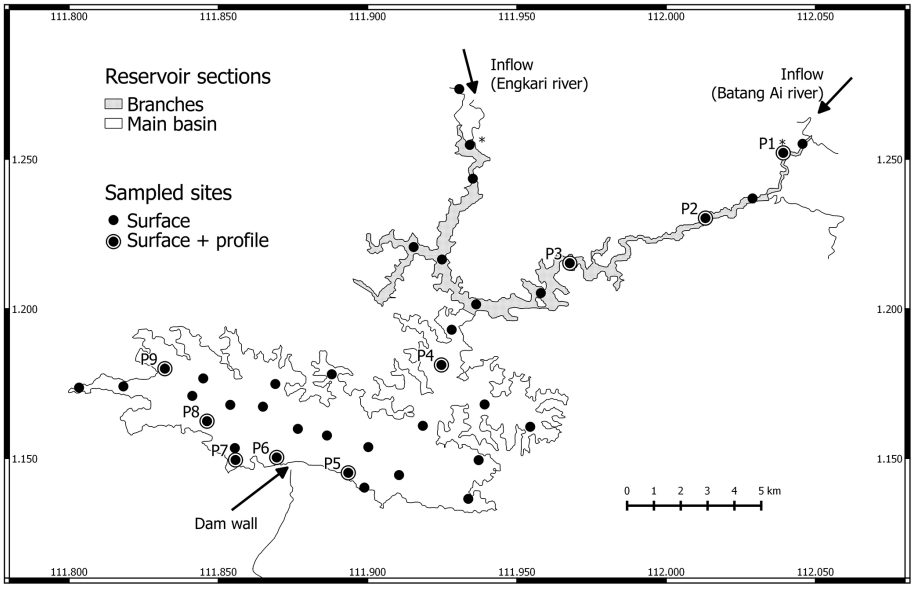

Figure 1. Map of Batang Ai reservoir with delimited sections (branches and main basin) and sampling points. * Represents sampling points at the branches' extremities.

as the reservoir branches (10.8 km^2, mean and max depths of 18 and 52 m respectively). The reservoir branches merge into the main basin of the reservoir (58.9 km^2, mean and max depths of 30 and 73 m respectively). Surface sampling was performed at 36 sites across the three study sections, and water column profile sampling (from 0 up to 32 m, each 0.5 to 3 m) was done at nine sites in the reservoir branches and main basin (Fig. 1). Sampling was repeated (with a few exceptions) during four campaigns: (1) 14 November to 5 December 2016 (November–December 2016), (2) 19 April to 3 May 2017 (April–May 2017), (3) 28 February to 13 March 2018 (February–March 2018), and (4) 12 to 29 August 2018 (August 2018).

2.2 Physical and chemical analyses

Water temperature, dissolved oxygen, and pH were measured using a multi-parameter probe (YSI model 600XLM-M) equipped with a depth gauge and attached to a 12 V submersible pump (Proactive Environmental Products model Tornado) for water sample collection. Concentrations of dissolved organic carbon (DOC), total phosphorus (TP), total nitrogen (TN), and chlorophyll *a* (chl *a*) were measured during all campaigns at all surface sampling sites (Fig. 1). Methods for these analyses are described in detail in Soued and Prairie (2020). Briefly, TP and chl *a* (extracted with hot ethanol) were analyzed via spectrophotometry, and TN and DOC (filtered at 0.45 µm) were measured on an Alpkem Flow Solution IV autoanalyzer and on a total organic carbon analyzer 1010-OI respectively.

For each site, we defined the depths of the thermocline and the top and bottom of the metalimnion based on measured temperature profiles using the R package rLakeAnalyzer (Winslow et al., 2018). The epilimnion was defined from the surface to the top of the metalimnion and was assumed to be a mixed layer.

2.3 Gas concentration, isotopic signature, and water–air fluxes

CO_2 and CH_4 gas concentrations and isotopic signatures ($\delta^{13}C$) were measured in duplicates at the surface at 36 sites and along vertical profiles at nine sites (P1 to P9, Fig. 1) using the headspace technique described in detail in Soued and Prairie (2020). In brief, sampling was done by equilibrating the water sample for 2 min with an air headspace inside a 60 mL syringe. The gas phase was then injected in a 12 mL pre-vacuumed airtight vial and analyzed on a gas chromatograph (Shimadzu GC-8A with a flame ionization detector) for gas concentrations and on a cavity ring-down spectrometer (CRDS) equipped with a small sample isotopic module (SSIM, Picarro G2201-i) for $\delta^{13}CO_2$ and $\delta^{13}CH_4$.

Surface gas flux data used in this study are described in more detail in Soued and Prairie (2020), a previous study on the C footprint of Batang Ai reservoir. Surface diffusive fluxes of CO_2 and CH_4 were measured at all surface sampling sites during each campaign. Flux rates were derived from linear changes in CO_2 and CH_4 concentrations in a static floating chamber (design described in Soued and Prairie, 2020 and IHA, 2010) connected in a closed loop to a portable gas analyzer (model UGGA, from Los Gatos Research). Measured gas concentrations, isotopic signature, and fluxes were spatially interpolated to the whole reservoir area by inverse distance weighting (given the absence of a suitable

variogram for kriging) using package gstat version 1.1-6 in the R version 3.4.1 software (Pebesma, 2004). Mean values were calculated for each campaign based on the interpolated maps (Soued and Prairie, 2020).

2.4 Horizontal GHG inputs

In order to estimate the external horizontal inputs of CO_2 and CH_4, we considered that the total volume of water inflow and outflow (discharge measured at the dam) were equal and equivalent to the mean of measured daily discharge (Q, in $m^3\,d^{-1}$) during each campaign (considering minimal changes in inflow and outflow rates during a campaign). The approach of using discharge as a measure of total water inflow has the advantage of integrating all external flow (rivers, lateral soils, and groundwater) as water inputs to the reservoir. However, the fraction of inflow feeding the reservoir surface vs. bottom layer and its average gas concentration can only be approximated based on measurements from the two main river inlets (Fig. 1) due to the lack of data on other lateral inflows. Given that part of the inflowing water is colder and denser than the reservoir surface layer, only a fraction of it enters the epilimnion of the reservoir branches, and the rest plunges into the hypolimnion. We estimated that fraction (f_{epi}) based on temperature profiles in the eastern river delta and branch (sites P1 and P2, Fig. 1), and we assumed it is representative of other water inflows to the reservoir. The areal rate of horizontal CO_2 and CH_4 inputs (H, in $mmol\,m^{-2}\,d^{-1}$) over each section of the reservoir were then calculated following Eq. (1):

$$H = \frac{C_{in}\,Q\,f_{epi}}{A}, \tag{1}$$

with A (m^2) the surface area of the reservoir section considered and C_{in} ($mmol\,m^{-3}$) the concentration of gas in the inflowing water. To estimate gas inputs from the inflows to the branches, C_{in} was considered to be the average of gas concentrations measured at the two upstream extremities of the branches (Fig. 1). To estimate gas inputs from the branches to the main basin, C_{in} was considered to be the gas concentrations measured at the confluence between the two branches (right upstream of the main basin).

2.5 Vertical GHG fluxes

We estimated CO_2 and CH_4 fluxes from the metalimnion to the epilimnion (V) based on the vertical gas diffusivity (K_z) and the gradient in gas concentration across the epilimnion–metalimnion interface using Eq. (2) (Wüest and Lorke, 2009):

$$V = K_z(C_{meta} - C_{epi}), \tag{2}$$

where C_{meta} and C_{epi} are the gas concentrations at the top of the metalimnion and at the bottom of the epilimnion respectively, measured at profile sites (P1 to P9, Fig. 1). K_z was derived from the following Eq. (3) (Osborn, 1980):

$$K_z = \Gamma\frac{\epsilon}{N^2}, \tag{3}$$

where Γ is the mixing ratio set to 0.2 (Oakey, 1982), ϵ is the dissipation rate of turbulent kinetic energy, and N^2 is the buoyancy frequency. N^2 was calculated from measured temperature profiles (YSI probe) using the function buoyancy.freq from the rLakeAnalyzer package (Winslow et al., 2018) in the R software (R Core Team, 2017). ϵ was derived from measured vertical shear microstructure profiles performed in the August 2018 campaign at all profile sites shown in Fig. 1 (except P1 due to floating logs). Shear profiles were measured with a high-frequency (512 Hz) MicroCTD profiler (Rockland Scientific) equipped with two velocity shear probes, two thermistors, tilt and vibration sensors, and a pressure sensor. At each site, the profiler was cast 10 times, five with an uprising configuration (from bottom to top of the water column) and five with a downward configuration (top to bottom), with a 4 min waiting time between profiles to allow water column disturbance to subside. Data quality check and ϵ calculation for each profile cast were performed with the ODAS v4.3.03 MATLAB library (developed by Rockland Scientific) based on Nasmyth shear spectrum (Oakey, 1982), with ϵ values averaged among the two shear probes and binned over 1–2 m segments along the profile. For each site, continuous ϵ profiles were interpolated by fitting a smooth spline through all ϵ values from replicate casts as a function of depth.

At the epilimnion–metalimnion interface (top of the metalimnion ±2 m), calculated ϵ averaged 7.7×10^{-9} (range from 3.4×10^{-9} to 1.6×10^{-8}) $m^2\,s^{-3}$ across all sites sampled with the MicroCTD, with no significant difference between the main basin and branch sites. In order to estimate vertical gas diffusion, we applied the latter ϵ average to Eqs. (2) and (3) for all measured gas profiles (except P1). The resulting V values for each gas were averaged across sites in the main basin and branches separately to derive estimates of V for each of these two reservoir sections.

2.6 Sediment GHG inputs

We calculated CO_2 and CH_4 inputs from the sediments to epilimnetic waters using gas profiles in sediment cores collected in April–May 2017 and February–March 2018 at seven sites (P1 to P3 in the reservoir branches and P4, P5, P7, and P9 in the main basin, Fig. 1). Sediment cores were collected using a Glew gravity corer attached to a 6 cm wide plastic liner. The liner was predrilled with 1 cm holes covered with electric tape at each centimetre up to 40 cm. Upon recovery of the sediment core, 3 mL tip-less syringes were inserted into each hole to extract sediments from each centimetre. The sediment content of each syringe was emptied into a 25 mL glass vial prefilled with 6 mL nano-pure water and immediately airtight sealed by a butyl rubber stopper crimped

with an aluminum cap. Glass vials were pressurized with 40 mL of ambient air using a plastic syringe equipped with a needle to pierce the rubber cap. Glass vials were shaken for 2 min for equilibration before extracting the gas with a syringe and injecting it into a pre-evacuated airtight vial for analysis of CO_2 and CH_4 concentrations and isotopic signatures as described above. Additionally, samples of the water overlaying the sediments ($\sim$ 1 cm above) were collected for similar analyses of CO_2 and CH_4.

Sediment CO_2 and CH_4 flux rates to the overlaying water column were derived from the vertical gradient of gas concentration measured in the sediment cores and overlaying water. The slope of CO_2 or CH_4 concentration as a function of depth (g, in $\mu mol\,L^{-1}\,m^{-1}$) was calculated for measured values in the first 5 cm of sediments and overlaying water. Most cores exhibited clear linear slopes (p value < 0.05 and $R^2_{adj} > 0.5$). In the few cases where a linear slope was not evident, g was replaced by the gradient between the mean gas concentration in the first 3 cm of sediments and the overlaying water. The sediment gas flux rate (S_f in $mmol\,m^{-2}\,d^{-1}$) was calculated with Eq. (4):

$$S_f = \frac{g \times d}{p}, \tag{4}$$

with d the diffusion coefficient set to $1.5 \times 10^{-5}\,cm^2\,s^{-1}$ (Donis et al., 2017) and p the sediment porosity assumed to be 2 % based on previous results in Batang Ai (Tan, 2015).

At an ecosystem scale, sediment CO_2 and CH_4 inputs to the water column (S) were estimated based on average and standard deviation values of sites located in each section of the reservoir (branches and main basin). For each section, mean sediment CO_2 and CH_4 flux rates were multiplied by the areal ratio of epilimnetic sediments (A_{epi}) vs. total water area (A_0). The latter ratio was calculated based on the hypsometric model (Ferland et al., 2014; Imboden, 1973) as shown in Eqs. (5) to (7):

$$q = \left(\frac{z_{max}}{z_{mean}}\right) - 1, \tag{5}$$

$$A_{epi} = A_0 \left(1 - \left(1 - \left(\frac{z_{epi}}{z_{max}}\right)\right)^q\right), \tag{6}$$

$$S = \frac{A_{epi}}{A_0} S_f, \tag{7}$$

with q a parameter describing the general bathymetric shape of the reservoir section, z_{max} and z_{mean} the maximum and mean depths respectively, and z_{epi} the mean depth of the epilimnion (8.0 and 10.5 m in the branches and main basin respectively).

Littoral sediments are known to be a source of CH_4 not only through diffusion but also via ebullition. While this emission pathway was found to be important in other reservoirs (Deemer et al., 2016), it is surprisingly low in Batang Ai, equaling less than 2 % of CH_4 surface diffusive emissions, and only 0.1 % of the reservoir total GHG footprint (Soued and Prairie, 2020). Therefore, sediment ebullition was considered negligible in the epilimnetic CH_4 budget of Batang Ai.

2.7 Metabolic rates

Net metabolic rates of CO_2 and CH_4 production in the epilimnetic water column were estimated with in situ incubations. Incubations were performed at five sites (P2 and P3 in the branches and P4, P5, and P7 in the main basin, Fig. 1). Water from 3 m deep was pumped into 5 L transparent glass jars with an airtight clamp lid. Before closing, jars were filled from the bottom and allowed to overflow and then sampled for initial CO_2 and CH_4 concentrations. Closed jars were fixed at 3 m to an anchored line at the sampling site and incubated in in situ temperature and light conditions for 22.0 to 24.2 h. Upon retrieval, samples of final CO_2 and CH_4 concentrations were collected from the jars. Volumetric daily rates of net CO_2 and CH_4 production were calculated based on the difference between final and initial gas concentrations rescaled to a 24 h period.

In addition to incubations, open-water high-frequency O_2 measurements were carried out to derive CO_2 metabolism on larger spatial and temporal scales. Rates of GPP, ER, and net ecosystem production (NEP) were estimated in the reservoir surface layer by monitoring and inverse modelling diel O_2 changes in the epilimnion. O_2 was measured at a 1 min interval using high-frequency O_2 and temperature sensors (model miniDOT from Precision Measurement Engineering), along with light sensors (model HOBO Pendant from Onset). Sensors were deployed in profile sites P1 to P3 in the branches and P4, P5, P7, and P9 in the main basin (Fig. 1). Note that not all sites were sampled in all sampling campaigns. Sensors were attached to an anchored line at a depth between 0.7 and 3 m and deployment time varied between 4 d and 2 weeks. Upon retrieval of the sensors, the first data quality check and selection were made based on the sensor internal quality index and visual screening. Rates of ecosystem metabolism were then estimated based on an open-system diel O_2 model (Odum, 1956), where change in O_2 concentration is a function of GPP, ER, and air–water gas exchange (K_{O_2}) following Eq. (8) (Hall and Hotchkiss, 2017):

$$\frac{dO_2}{dt} = \frac{GPP}{z_{epi}} + \frac{ER}{z_{epi}} + K_{O_2}\,(O_{2sat} - O_2), \tag{8}$$

with O_{2sat} the theoretical O_2 concentration at saturation considering the in situ temperature and atmospheric pressure, and O_2 is the actual measured O_2 concentration in the water. A detailed description of the model equations can be found in Hall and Hotchkiss (2017). Daily estimates of GPP, ER, and K_{600} (based on K_{O_2}) were derived by maximum likelihood fitting of the data to the model in Eq. (8) using the R package StreamMetabolizer (Appling et al., 2018). Note that even though the package used was originally developed for streams, it is easily transferable to lakes given that the model

used (Eq. 8) is generalized for all water bodies, with the parameter z_{epi} describing the depth of a mixed water column of either a lentic or lotic system and with the K_{600} estimate relying only on data fitting to the model and not on system type. In some cases, where the best predicted K_{600} was negative, the fitting process was rerun with a user-defined positive K_{600}, either equal to a value estimated for the previous or subsequent day at the same site (range of 0.03–0.96 d^{-1}) or fixed to 0.1 d^{-1} (if there is no other available estimate). When considering the epilimnion depth, predicted values of K_{600} translate into a first to third quantile range of 1.17 to 5.55 $m\,d^{-1}$, which is similar to the range of K_{600} values back-calculated from surface gas flux measurements with the floating chamber technique. A final selection of daily metabolic estimates was done based on the model goodness of fit assessed by calculating Pearson correlation coefficient between modelled and measured O_2 values and discarding days with a correlation lower than 0.9. Based on GPP and ER estimates, we calculated daily NEP as the balance between these two processes, and we converted it to net CO_2 production rate by assuming an $O_2 : CO_2$ metabolic quotient of 1.

Areal metabolic rates were derived by integrating volumetric rates over the depth of the epilimnion. Average estimates of areal metabolic rates per campaign were obtained for the branches and main basin by first averaging data within each site and then across sites for each reservoir section. Note that one value derived from incubations was excluded from the calculation of the average net CH_4 production rate in the branches due to its high value of initial CH_4 concentration (an order of magnitude higher than in all other incubations and all epilimnetic data from this site). The high CH_4 concentration, unrepresentative of real conditions, was probably caused by CH_4 contamination during sampling and triggered a high oxidation rate that would overestimate the real ecosystem average rate if included.

2.8 Epilimnetic GHG budgets

Areal rates of horizontal, vertical, sediment, and metabolic inputs were combined into a sum of sources and sinks and compared to the rate of surface gas flux for each gas in each reservoir section. A mean and standard error were calculated for every component of the budgets based on measurements averaged across sites and/or sampling campaigns in order to obtain ecosystem-scale estimates of the component means and uncertainties. In the case of CO_2 metabolism, the ecosystem-scale average was calculated as the mean of the two average values derived from the incubation and diel O_2 monitoring methods. For every component, density curves were derived considering a normal distribution based on the mean and its standard error in order to visualize the relative magnitude and uncertainty of each ecosystem-scale areal rate (Fig. 3).

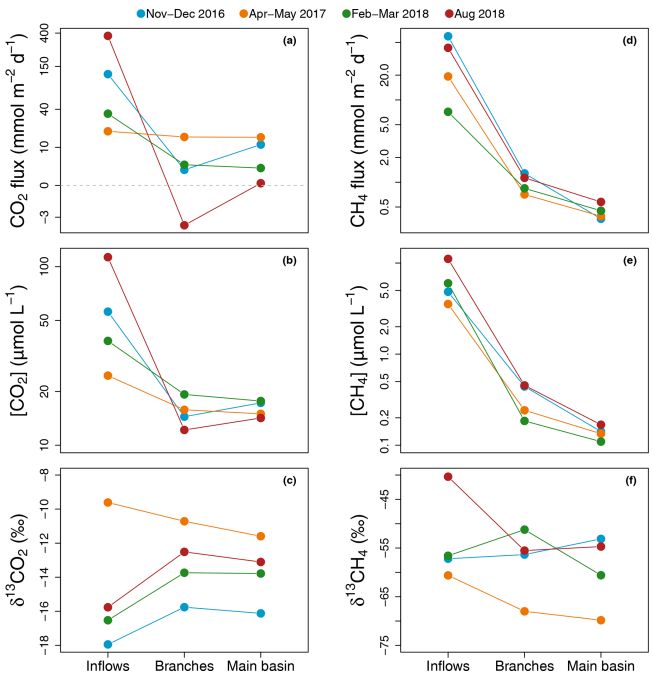

Figure 2. Average of spatially interpolated surface CO_2 **(a–c)** and CH_4 **(d–f)** fluxes **(a, d)**, concentrations **(b, e)**, and isotopic signatures **(c, f)** along the hydrological continuum from the reservoir inflows to the main basin for each sampling campaign.

3 Results

3.1 Physical and chemical properties

Surface water temperature exhibited a marked increase from the inflows to the branches, averaging 27.1 and 30.7 °C respectively (Table 1). There was no difference in surface water temperature between the branches and the main basin. The depth of the epilimnion tended to increase and become more stable along the water flow, going from 1.3 (±1.6) m in the Batang Ai River delta to 8.0 (±2.3) m in its branch and 10.6 (±1.7) m in the main basin (Table 1). Light penetration exhibited the same spatial pattern, with an increasing Secchi depth along the water flow averaging 1.3, 5.1, and 5.5 m in the inflows, branches, and main basin respectively (Table 1). All sections of the study system exhibited oligotrophic water properties (Table 1).

3.2 Surface GHG concentrations, fluxes, and isotopic signatures

Surface CO_2 and CH_4 patterns are summarized in Fig. 2, presenting campaign averages of spatially interpolated gas concentration, flux, and isotopic signature along the different reservoir sections. Despite the temporal variability, the gas patterns along the water flow are robust, remaining similar throughout time (Fig. 2).

Table 1. Mean (±SD) of physical and chemical variables measured at the surface of the three reservoir sections.

Variables	Units	Inflows	Branches	Main basin
z_{epi}	m	1.3 (±1.6)	8 (±2.3)	10.6 (±1.7)
Secchi	m	1.2 (±0.9)	5.1 (±1.2)	5.5 (±1.2)
Temperature	°C	27.1 (±2.5)	30.7 (±0.5)	30.6 (±0.5)
pH		6.5 (±0.3)	7.2 (±0.2)	7.2 (±0.2)
O_2	%	94.9 (±7.7)	102.7 (±4.5)	99.3 (±4.8)
DOC	$mg\,L^{-1}$	0.8 (±0.4)	0.9 (±0.2)	0.9 (±0.2)
TP	$\mu g\,L^{-1}$	20.7 (±7.6)	6.2 (±1.7)	5.8 (±2.6)
TN	$mg\,L^{-1}$	0.14 (±0.04)	0.12 (±0.04)	0.1 (±0.03)
Chl *a*	$\mu g\,L^{-1}$	2.1 (±1.7)	1.7 (±1)	1.2 (±0.5)

Average CO_2 air–water flux and surface concentration were systematically higher in the inflows (mean [range]: 135.3 [18.9–368.8] $mmol\,m^{-2}\,d^{-1}$ and 58.0 [24.5–113.0] $\mu mol\,L^{-1}$ respectively) compared to the branches (4.7 [−3.4–15.2] $mmol\,m^{-2}\,d^{-1}$ and 15.4 [12.2–19.3] $\mu mol\,L^{-1}$) and main basin (7.5 [0.3–15.1] $mmol\,m^{-2}\,d^{-1}$ and 16.0 [14.2–17.7] $\mu mol\,L^{-1}$) (Fig. 2a and b). Surface CO_2 concentration in the reservoir (branches and main basin) was most strongly correlated inversely with water temperature ($R^2_{adj} = 0.22$, p value < 0.001, Fig. S1a and Table S1 in the Supplement). Except for the April–March 2017 campaign, there was a modest increase (2.2‰ to 3.3‰) in surface $\delta^{13}CO_2$ towards more enriched values from the inflows to the branches (Fig. 2c).

Similarly, surface CH_4 flux and concentration continually decreased along the water channel, being an order of magnitude higher in the inflows compared to the branches and about twice as high in the branches compared to the main basin (Fig. 2d and e). Of all measured water properties, TN was the most strongly linked to reservoir surface CH_4 concentration ($R^2_{adj} = 0.14$, p value < 0.001, Fig. S1b and Table S1). In the main basin, surface CH_4 concentration significantly decreased with distance to shore in November–December 2016 ($R^2_{adj} = 0.54$, p value < 0.001), but this correlation was weaker ($R^2_{adj} \leq 0.13$, p value ≥ 0.03) during other sampling campaigns (Fig. 6a). Surface $\delta^{13}CH_4$ values varied widely, between −83.3 and −47.6‰, but did not show a consistent spatial pattern (Fig. 2f) apart from a positive correlation with distance to shore in the main basin in November–December 2016 ($R^2_{adj} = 0.29$, p value $= 0.01$, Fig. 6b).

The degree of coupling between CO_2 and CH_4 followed a clear spatial pattern. While CO_2 and CH_4 surface concentrations were strongly linked in the inflows ($R^2_{adj} = 0.54$, p value $= 0.006$), they became only weakly correlated in the branches ($R^2_{adj} = 0.17$, $p = 0.005$) and not correlated at all in the main basin ($R^2_{adj} = 0.01$, p value $= 0.11$) (Fig. S2 in the Supplement).

3.3 Horizontal GHG flow

Horizontal inputs from the inflows to the surface layer of the branches were estimated to vary between 0.34–0.71 $mol\,s^{-1}$ for CO_2 and 0.02–0.25 $mol\,s^{-1}$ for CH_4. When expressed as areal rates over the branches (to facilitate comparison with other components), horizontal inputs amounted to 2.7–5.7 and 0.16–1.97 $mmol\,m^{-2}\,d^{-1}$ for CO_2 and CH_4 respectively (Tables S2 and S3 in the Supplement). These values are of the same order of magnitude as surface fluxes calculated in the branches (Fig. 3a and c, Tables S2 and S3). However, the effect of horizontal inputs faded spatially, with much lower inputs from the branches to the main reservoir basin, averaging 0.31 and 0.004 $mmol\,m^{-2}\,d^{-1}$ for CO_2 and CH_4 respectively (Fig. 3b and d and Tables S2 and S3). For CH_4, this fits spatial and temporal surface flux measurements, being systematically higher in the branches and maximal during the two sampling campaigns with the highest recorded horizontal inputs from the inflows (Table S3). In contrast, CO_2 surface flux was typically lower (sometimes negative) in the branches compared to the main basin, despite substantial riverine inputs to the branches (Table S2).

3.4 Vertical GHG inputs

Vertical fluxes depend on the gas diffusivity and concentration gradient. Gas diffusivity is a function of the strength of stratification (N^2) and energy dissipation rate (ϵ). Measured values of N^2 and ϵ varied widely, from 5.9×10^{-5} to $2.3 \times 10^{-3}\ s^{-2}$ and from 3.4×10^{-9} to $1.6 \times 10^{-8}\ m^2\,s^{-3}$ respectively, but with no clear differences between the reservoir branches and main basin (Fig. S3a and b in the Supplement). Similarly, CO_2 and CH_4 concentration gradients varied substantially in both space and time (from −18.4 to 94.3 $\mu mol\,L^{-1}\,m^{-1}$ for CO_2 and −0.19 to 0.4 $\mu mol\,L^{-1}\,m^{-1}$ for CH_4). CO_2 concentration generally increased from the epilimnion to the metalimnion as a result of the respiratory CO_2 buildup in the deep layer. On rare occasions, an inverse gradient was observed, possibly due to autotrophic activity in the metalimnion. For CH_4, metalimnion-to-epilimnion concentration gradients were generally modest, averaging

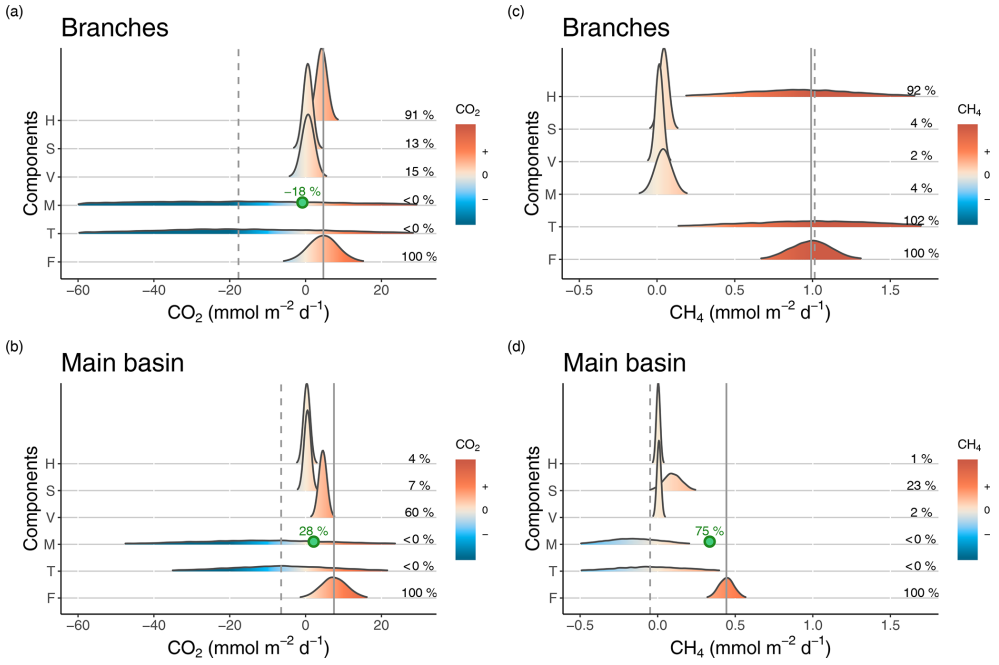

Figure 3. Density distributions of the different components of CO_2 **(a, b)** and CH_4 **(c, d)** surface budgets in the reservoir branches **(a, c)** and main basin **(b, d)**. Components are as follows. H: horizontal flow inputs; S: sediment inputs; V: vertical inputs; M: net metabolism (average of the incubation and diel O_2 monitoring methods); T: sum of all estimated sources and processes in the surface layer; F: measured surface fluxes. Density curves are based on simulated normal distributions using the mean and standard error of each component. The x axes represent the areal rate of CO_2 or CH_4, and the colour scale indicates the sign of the rate. Mean values of the fraction of each component (%) relative to the mean surface flux (F) are reported on the right side in each panel. The solid and dashed grey lines represent the means of F and T respectively. In panels (**a**), (**b**), and (**d**), the point and percentage in green represent the hypothetical value of the M rate (the most uncertain component) and its corresponding fraction (as a percentage of F) that are needed to close the budget (to obtain $T = F$).

$0.04\,\mu mol\,L^{-1}\,m^{-1}$, and even negative in one-third of the profiles, leading to the diffusion of epilimnetic CH_4 toward deeper layers instead of the reverse. The low to negative CH_4 vertical flux results from a highly active methanotrophic layer reducing CH_4 concentration in the metalimnion, as evidenced by the strong enrichment effect observed in $\delta^{13}CH_4$ profiles (Fig. S4 in the Supplement). The combination of vertical diffusivity and gas concentration gradients resulted in vertical fluxes averaging 3.4 (-1.8 to 20.5) $mmol\,m^{-2}\,d^{-1}$ for CO_2 and 0.01 (-0.01 to 0.09) $mmol\,m^{-2}\,d^{-1}$ for CH_4, with no significant differences between the reservoir branches and main basin (Fig. S3).

3.5 GHG inputs from littoral sediments

Areal sediment gas fluxes ranged from 1.2 to 4.0 and -0.29 to 1.10 $mmol\,m^{-2}\,d^{-1}$ for CO_2 and CH_4 respectively (Fig. S5 in the Supplement), in the range of previously reported values in lakes and reservoirs (Adams, 2005; Algesten et al., 2005; Gruca-Rokosz and Tomaszek, 2015; Huttunen et al., 2006). Sediment fluxes were not different in the branches vs. the main basin for both CO_2 (mean of 2.2 vs. 2.4 $mmol\,m^{-2}\,d^{-1}$) and CH_4 (mean of 0.17 vs. 0.48 $mmol\,m^{-2}\,d^{-1}$) (Fig. S5). Applying measured averages to the area of epilimnetic sediments in each section yields estimates of sediment inputs to the epilimnion of 0.6 ($\pm$0.03) and 0.5 ($\pm$0.11) $mmol\,m^{-2}\,d^{-1}$ for CO_2 and 0.04 ($\pm$0.02) and 0.10 ($\pm$0.06) $mmol\,m^{-2}\,d^{-1}$ for CH_4 in the branches and main basin respectively (Fig. 3 and Tables S2 and S3). These inputs from littoral sediments likely represent an upper limit since they are based on deep pelagic sediment cores (littoral area were too compact for coring), where a higher organic matter accumulation and degradation is expected (Blais and Kalff, 1995; Soued and Prairie, 2020). Even as upper estimates, the calculated rates of sediment GHG inputs remain a relatively modest fraction of the average emissions to the atmosphere for the branches and main basin for both CO_2 (13 % and 7 % respectively) and CH_4 (4 % and 23 % respectively) (Tables S2 and S3).

3.6 Metabolism

3.6.1 CO_2 metabolism

Estimated GPP and ER rates based on diel O_2 monitoring ranged from 3.6 to 34.5 $\mu mol\,L^{-1}\,d^{-1}$ and from 5.8 to 29.5 $\mu mol\,L^{-1}\,d^{-1}$ respectively (Fig. 4a), which is well within the range of reported rates for oligotrophic systems (Bogard and del Giorgio, 2016; Hanson et al., 2003; Solomon

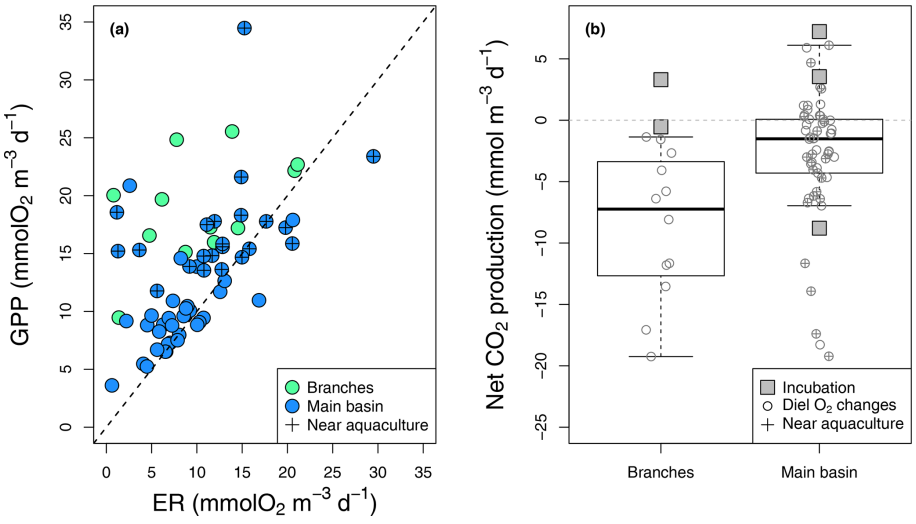

Figure 4. Epilimnetic daily GPP vs. ER rates **(a)** derived from diel O_2 changes in the reservoir branches and main basin (including sites near aquacultures), with the 1 : 1 line (dotted). **(b)** Boxplots of the corresponding rates of CO_2 NEP in the branches and main basin, with box bounds, whiskers, solid line, open circles, and squares representing the 25th and 75th percentiles, the 10th and 90th percentiles, the median, single data points (diel O_2 method), and incubation-derived rates respectively.

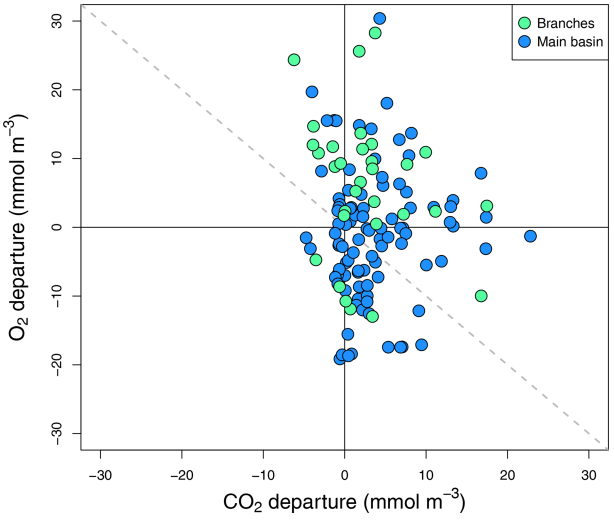

Figure 5. Surface O_2 vs. CO_2 departure from saturation for all sampled surface sites in the reservoir main basin and branches across all sampling campaigns.

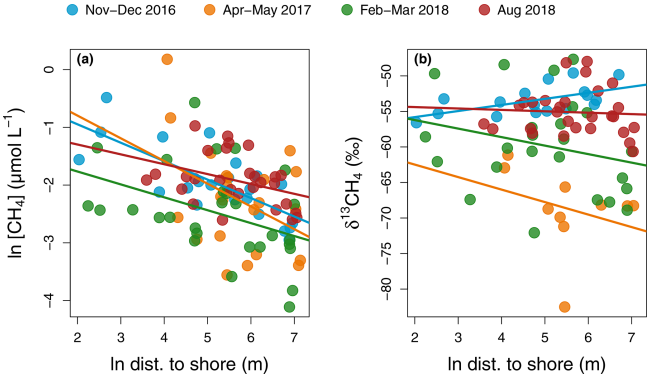

Figure 6. Regression of CH_4 concentration **(a)** and isotopic signature **(b)** as a function of distance to shore in each sampling campaign in the main reservoir basin. For CH_4 concentration, regressions lines have the following statistics in order of sampling: p values: < 0.001, 0.06, 0.03, and 0.05 and R^2_{adj}: 0.54, 0.13, and 0.11. For $\delta^{13}CH_4$, all regressions had p values > 0.2 except for the November–December 2016 campaign with a p value $= 0.01$ and $R^2_{adj} = 0.29$.

et al., 2013). As expected, GPP and ER rates were correlated ($R^2_{adj} = 0.23$, p value < 0.001, Fig. 4a), with photosynthesis stimulating the respiration of produced organic matter. In most cases, GPP exceeded ER, especially in the branches and near aquacultures (Fig. 4a), where higher nutrients (TP and TN) and chl *a* concentrations were measured (Table 1). Daily metabolic rates showed no correlation with mean daily rain or light (Kendall rank correlation p value > 0.1).

In the reservoir branches, results from the diel O_2 monitoring method suggested systematic net CO_2 uptake ranging from -19.2 to $-1.4\,\mu mol\,L^{-1}\,d^{-1}$, whereas results from two incubations were slightly above that range (-0.5 to $3.3\,\mu mol\,L^{-1}\,d^{-1}$) (Fig. 4b). In the main basin, incubation results ranged from -8.8 to $7.2\,\mu mol\,L^{-1}\,d^{-1}$, while the diel O_2 technique captured a wider variability in net CO_2 metabolic rates from -19.2 to $6.1\,\mu mol\,L^{-1}\,d^{-1}$, with an estimated CO_2 uptake in 39 out of 54 cases (Fig. 4b). Areal net CO_2 metabolic rates, as the average of the two

methods, yielded an ecosystem-scale estimate of −23.2 and $-11.8\,\mathrm{mmol\,m^{-2}\,d^{-1}}$ in the reservoir branches and main basin respectively (Table S2).

To complement the metabolic rate data, surface O_2 and CO_2 departure from saturation was examined in both reservoir sections. O_2 oversaturation was observed in 44 % of cases in the main basin and 81 % in the branches (Fig. 5), which corresponds with the spatial patterns of net metabolic rates (Fig. 4b). CO_2 oversaturation was also widespread (74 % of cases), making many sampled sites oversaturated in both O_2 and CO_2 (55 % in the branches and 32 % in the main basin, Fig. 5).

3.6.2 CH_4 metabolism

Net metabolic CH_4 rates (from incubations) ranged from -0.026 to $0.078\,\mathrm{\mu mol\,L^{-1}\,d^{-1}}$, indicating that the CH_4 balance in the epilimnion of Batang Ai varied from net oxidation to net production (Table S3). CH_4 metabolic rates measured in Batang Ai are within the range of values observed in other systems for oxidation (Guérin and Abril, 2007; Thottathil et al., 2019) and production (Bogard et al., 2014; Donis et al., 2017). No temporal or spatial (branches vs. main basin) differences in net metabolic CH_4 rate were detected due to a high variability and limited data points.

3.7 Ecosystem-scale GHG budgets

Estimated sources and sinks of CO_2 and CH_4 were collated into a budget to evaluate their relative impact on epilimnetic gas concentration and to assess whether their sum matches the measured surface gas fluxes in each section of the reservoir. Figure 3 depicts such reconstruction of the epilimnetic CO_2 and CH_4 budgets in Batang Ai as well as the uncertainty limits of each component. While each process varied in time, their relative importance in driving surface fluxes was generally similar from one sampling campaign to another (Tables S2 and S3).

3.7.1 CO_2 budget

For CO_2, epilimnetic sediment inputs had a small contribution, being typically an order of magnitude lower than measured surface fluxes in both sections of the reservoir (Fig. 3a and b and Table S2). Vertical CO_2 inputs from lower depths on the other hand contributed substantially to surface fluxes in the branches and especially in the main basin (mean of 0.7 and $4.5\,\mathrm{mmol\,m^{-2}\,d^{-1}}$ respectively, Fig. 3a and b and Table S2), indicating that hypolimnetic processes impact surface emissions despite the permanent stratification. Horizontal inputs of CO_2 averaged $4.3\,\mathrm{mmol\,m^{-2}\,d^{-1}}$ in the branches; however, they decreased by an order of magnitude when reaching the main basin (mean of $0.3\,\mathrm{mmol\,m^{-2}\,d^{-1}}$). Thus, direct CO_2 inputs from the inflows notably increase surface flux rates in the reservoir branches but only minimally in the main basin. Net CO_2 metabolism was surprisingly variable (switching from negative to positive NEP on a daily timescale), thus making it difficult to derive a sufficiently precise ecosystem-scale estimate to close the epilimnetic budget (Fig. 3a and b), despite high sampling resolution ($n = 66$ daily metabolic rates). Including the metabolism substantially shifts the mean of the CO_2 epilimnetic budget (sum of sources and sinks) to a negative value and drastically increases its uncertainty (Fig. 3a and b and Table S2), reflecting a potentially important but poorly resolved role of metabolism in the budget because of its variability. However, given that metabolism acts more likely as a CO_2 sink on average, our best assessment suggests that vertical transport from deeper layers is the main source sustaining surface CO_2 outflux in the main basin of Batang Ai.

3.7.2 CH_4 budget

In contrast with CO_2, vertical transport was the smallest source of CH_4 to the epilimnion, contributing to only 2 % of surface fluxes in both reservoir sections (Fig. 3c and d and Table S3). In the branches, sediment inputs and net CH_4 metabolic rates were both relatively low (mean of 0.04 ± 0.02 and $0.04 \pm 0.05\,\mathrm{mmol\,m^{-2}\,d^{-1}}$) and had little impact on the budget, corresponding each to 4 % of surface fluxes in that section (Fig. 3c and Table S3). On the other hand, horizontal inputs were the dominant and most variable source sustaining CH_4 emissions in the branches, where the epilimnetic mass balance closed almost perfectly (Fig. 3c and Table S3). Despite being the main CH_4 source in the branches, horizontal transport was a negligible component in the main basin (1 % of the flux, Fig. 3d and Table S3). Instead, sediment inputs played a larger role in that section, with a mean of 0.10 (±0.06) $\mathrm{mmol\,m^{-2}\,d^{-1}}$, fuelling 23 % of surface emissions in the main basin (Fig. 3d and Table S3). As with CO_2, the most variable CH_4 component of the mass balance in the main basin was the net metabolism within the epilimnion (mean of $-0.16 \pm 0.19\,\mathrm{mmol\,m^{-2}\,d^{-1}}$). Considering all sources, the CH_4 budget indicates a deficit of $0.34\,\mathrm{mmol\,m^{-2}\,d^{-1}}$ to explain measured surface emissions in the main basin (Fig. 3d and Table S3).

4 Discussion

Our results have highlighted both the importance and the challenges associated with simultaneously quantifying all the components of the epilimnetic CO_2 and CH_4 budgets, particularly in a hydrologically complex reservoir system. While mass fluxes (hydrological, sedimentary, and air–water fluxes) are relatively easy to constrain, internal C processing, namely the net metabolic balances between production and consumption of CO_2 and CH_4, is highly dynamic in both time and space, leading to significant uncertainties when extrapolated to the ecosystem scale. In many studies, some components are only inferred by difference. While convenient from

a mass balance perspective, we argue that assessing all components together is necessary to clearly identify knowledge gaps as well as sources of uncertainty.

4.1 Spatial dynamics of CO_2 and CH_4

The decrease in gas concentration and air–water fluxes along the hydrological continuum observed across sampling campaigns and for both CH_4 and CO_2 reflects a robust spatial structure of the gases. Concurrently, estimates of the horizontal GHG inputs show a clear and consistent spatial pattern: high in the branches but negligible in the main basin. A temporal effect of riverine inputs was also observed as the two sampling campaigns with the highest horizontal CH_4 inputs coincided with the highest CH_4 emissions in the branches (Table S3). All these results concord with a progressively reduced influence of direct GHG catchment inputs and greater preponderance of internal processes along the hydrological continuum as observed in river networks (Hotchkiss et al., 2015) and in lakes and reservoirs (Chmiel et al., 2020; Loken et al., 2019; Paranaíba et al., 2018; Pasche et al., 2019).

For CO_2, the sharpest change in surface metrics (concentration, flux, and isotopic signature) was observed between the inflows and the reservoir branches (Fig. 2a–c). Despite large riverine inputs (Table S2), the branches exhibited low CO_2 concentration and fluxes as well as an increase in $\delta^{13}CO_2$ matching with high GPP values (Figs. 2a–c and 4a). This may reflect increased light availability for phytoplankton when transitioning from the turbid inflows to the reservoir branches (higher Secchi depth, Table 1), a pattern previously reported in other reservoirs (Kimmel and Groeger, 1984; Pacheco et al., 2015; Thornton et al., 1990). While the branch areas are often associated with high CO_2 outflux due to riverine inputs (Beaulieu et al., 2016; Paranaíba et al., 2018; Pasche et al., 2019; Roland et al., 2010; Rudorff et al., 2011), they are occasionally observed to have low air–water flux due to simultaneous nutrient inputs (Loken et al., 2019; Paranaíba et al., 2018; Wilkinson et al., 2016). In Batang Ai, inflows have a high ratio of nutrients (TP and TN) to DOC compared to the reservoir branches (Table 1), providing higher inputs of nutrients relative to organic matter and thus likely stimulating primary production more than respiration. This hypothesis is consistent with a higher GPP–ER ratio and mean chl *a* concentrations measured in the branches compared to the main basin (Fig. 4a and Table 1). The variability of CO_2 concentration within the reservoir (branches and main basin) was negatively correlated to temperature, likely due to its effect on GPP (Bogard et al., 2020). This further highlights the important role of primary production in modulating CO_2 dynamics throughout the reservoir and particularly in the branches.

The correlation between surface CH_4 and TN in the reservoir suggests that primary production may also affect CH_4 dynamics. Nutrient content was shown in previous studies to enhance CH_4 production in the sediments (Beaulieu et al., 2019; Gebert et al., 2006; Isidorova et al., 2019) and in the oxic water column (Bogard et al., 2014), through its link with algal production and decomposition. However, CH_4 concentration and flux variability were strongly driven by a spatial–hydrological structure, gradually decreasing from the inflows to the main basin. This likely reflects the combined effect of terrestrial inputs and a decreasing contact of water with sediments along the water channel. Surface $\delta^{13}CH_4$ signatures varied substantially but without a consistent spatial pattern (Fig. 2f), indicating that the surface CH_4 pool is shaped by multiple sources and processes (metabolism, riverine, and sediment inputs) varying through space and time.

The changing relative contribution of sources and processes shaping surface CO_2 and CH_4 concentrations varies with the system hydro-morphology, from the inflows to the main reservoir basin, and leads to a progressive decoupling between the two gases along the continuum (Fig. S2). The observed CO_2 and CH_4 coupling in the inflows and branches is associated with a common catchment source, as previously reported in other systems including soil–water (Lupon et al., 2019), streams (Rasilo et al., 2017), and lake and reservoir inflow areas (Loken et al., 2019; Natchimuthu et al., 2017; Paranaíba et al., 2018). Indeed, horizontal inputs are the main source of both CO_2 and CH_4 in the upstream reaches of Batang Ai, accounting on average for 91 % and 92 % of their respective surface outflux in the branch section (Fig. 3a and c and Tables S2 and S3). The hydro-morphometry of these channels can explain the large impact of horizontal inputs in the branch section, which is characterized by a relatively small ratio of water to catchment area and a direct connection to the major river inflows, creating a strong link between the catchment and the branches. However, when reaching the main basin, this link weakens due to a longer distance from river inflows and the dilution of horizontal inputs in a larger water volume. Thus, in the main basin, CO_2 and CH_4 are mostly driven by internal sources, diverging between the two gases, with vertical inputs from the bottom layer supporting on average 60 % of CO_2 compared to 2 % of CH_4 fluxes, while sediment inputs sustained 7 % vs. 23 % of CO_2 and CH_4 fluxes respectively in that section. This decoupling partly results from the two gases having distinct metabolic pathways: mainly aerobic for CO_2 and anaerobic for CH_4, leading to their sources and sinks being spatially disconnected in the main basin. Consequently, sediments being a mostly anaerobic environment are a more important source of CH_4 relative to CO_2, while the metalimnetic layer being oxic–hypoxic acts as a sink of CH_4 and source of CO_2 via aerobic CH_4 oxidation (Fig. S4). Overall, the spatial patterns reported here highlight the hydrodynamic zonation common in reservoirs and its diverging effect on CO_2 vs. CH_4 cycling.

4.2 CO_2 metabolism

Our observation that GPP often exceeded ER (Fig. 4a) was not unexpected given the very low DOC concentration (<

$1\,mg\,L^{-1}$). Previous work has reported that DOC $> 4\,mg\,L^{-1}$ is required to sustain persistent net heterotrophy and CO_2 evasion (Hanson et al., 2003; Prairie et al., 2002). Throughout the reservoir, we found high day-to-day variability in both ER and GPP, but with no apparent link to weather data (light and rain, data not shown). The absence of such a link at a daily timescale has been previously reported (Coloso et al., 2011), while other studies associated daily variations in metabolism with changes in water inflows carrying nutrients (Pacheco et al., 2015; Staehr and Sand-Jensen, 2007) or thermocline stability regulating hypolimnetic water incursions to the epilimnion (Coloso et al., 2011). Such variations in thermocline depth are thought to be more common in warm tropical systems (Lewis, 2010) and were observed across sampling campaigns in Batang Ai, especially in the branches where the depth of the mixed layer varied considerably (SD = 2.3 m, Table 1). Hence, hydrological and physical factors may regulate spatial and daily patterns of GPP and ER rates in Batang Ai through their influence on nutrient dynamics.

The accuracy of rates derived from diel O_2 monitoring partly depends on the respiratory and photosynthetic quotients (RQ and PQ) assumed for the conversion of metabolic rates from O_2 to CO_2. A quotient differing from the assumed 1 : 1 ratio can lead to an under- or overestimation of net CO_2 production. The fact that net CO_2 metabolic rates were on average higher in incubations, based on direct CO_2 measurements compared to diel O_2 monitoring (Fig. 4b and Table S2), hints at a deviation of the metabolic quotients from unity in Batang Ai. Additionally, surface O_2 vs. CO_2 concentrations shows that the departure of these gases from saturation varies widely around the expected $1 : -1$ line, with many surface samples oversaturated in both O_2 and CO_2, especially in the branches (Fig. 5). This indicates an excess O_2 and/or CO_2 that can be due to a PQ and/or a RQ higher than 1 or to external CO_2 inputs to the epilimnion (Vachon et al., 2020), for instance from the inflows or the bottom layer (Table S2). Metabolic quotients have been shown to vary widely, depending on the type and magnitude of photochemical and biological reactions at play (Berggren et al., 2012; Lefèvre and Merlivat, 2012; Vachon et al., 2020; Williams and Robertson, 1991). For instance, CH_4 oxidation and production, evidently occurring in Batang Ai's epilimnion (Tables S2 and S3), diverge from the metabolic $O_2 : CO_2$ ratio of 1, with CH_4 oxidation consuming 2 mol of O_2 for each mole of CO_2 produced and acetoclastic methanogenesis producing CO_2 without O_2 consumption. Even though net CH_4 processing rates are a minor portion of the epilimnetic C cycling in Batang Ai (1–2 orders of magnitude lower than CO_2 metabolic rates, Tables S2 and S3), these reactions (and other unmeasured processes) have the potential to alter the $O_2 : CO_2$ metabolic quotient at an ecosystem scale. The lack of direct measurements of metabolic quotients in Batang Ai adds uncertainty to the net CO_2 metabolism estimates based on O_2 data. The observed decoupling of O_2 and CO_2 metabolism in Batang Ai highlights the need for a deeper understanding of the biochemical reactions occurring in the epilimnion and their effect on metabolic quotients.

Overall, our results from Batang Ai reservoir point to water column metabolism as both a key process in the CO_2 epilimnetic budget and a challenging one to estimate at an ecosystem scale (Fig. 3a and b). Improving this requires a better mechanistic knowledge of the physical and biochemical processes at play and how they interact to shape NEP.

4.3 CH_4 metabolism

Incubation results exhibited a wide range of net CH_4 metabolism: from net oxidation to net production. CH_4 oxidation is known to be highly dependent on CH_4 availability and is optimal in low-oxygen and low-light conditions (Borrel et al., 2011; Thottathil et al., 2018, 2019), whereas CH_4 production in the oxic water is still poorly understood but has been frequently linked to phytoplankton growth (Berg et al., 2014; Bogard et al., 2014; Lenhart et al., 2016; Wang et al., 2017). A large variability in results exists among the studies that have assessed the net balance of CH_4 metabolism in the water column, with some studies reporting pelagic CH_4 production as a largely dominant process (Donis et al., 2017) while others find no trace of it (Bastviken et al., 2008). Based on spatial patterns of surface CH_4 concentration and isotopic signature with distance to shore, DelSontro et al. (2018b) showed that, in 30 % of their studied temperate lakes, CH_4 oxidation was dominant vs. 70 % dominated by net pelagic production. In Batang Ai, surface $\delta^{13}CH_4$ values were highly variable (-82.5 ‰ to -47.7 ‰) but mostly uncorrelated with distance to shore, except a positive correlation indicative of oxidation in November–December 2016 ($R^2_{adj} = 0.29$, p value $= 0.01$, Fig. 6b) coinciding with a strong inverse pattern for CH_4 concentration ($R^2_{adj} = 0.54$, p value < 0.001, Fig. 6a). This suggests a temporal shift in processes driving surface CH_4 patterns. Also, some measured surface $\delta^{13}CH_4$ values were lower than the mean $\delta^{13}CH_4$ from the sediments (-66.0 ‰, unpublished data), suggesting another highly depleted source of pelagic CH_4 in the system. This is in line with water incubation results often showing positive net CH_4 production (Table S3). When reported as mean areal rates, CH_4 metabolism ranged from net consumption to net production of CH_4 (-0.29 to $0.94\,mmol\,m^{-2}\,d^{-1}$), which reflects its potential in having a high impact, either positive or negative, on the epilimnetic CH_4 budget at the reservoir scale (Fig. 3d and Table S3). Results in Batang Ai show that the net balance of CH_4 metabolic processes varies widely even within a single system. However, the factors regulating this balance remain largely unknown. Investigating such factors constitute a key step in resolving CH_4 budgets in lakes and reservoirs.

4.4 Epilimnetic GHG budgets

For CO_2, measured surface fluxes in both reservoir sections fall in the range of possible values estimated by the sum of epilimnetic processes and their uncertainties (Fig. 3a and b and Table S2). However, the averages of those two terms differ substantially, due to negative values of metabolism shifting the mean of the mass balance towards net CO_2 consumption whereas, on average, surface out-flux was measured from the reservoir. This discrepancy indicates either a missing source of CO_2 in the budget or the underestimation of one of the processes. While lateral groundwater input is a potential source not explicitly considered, it is probably modest given the small ratio of littoral area to epilimnion volume, and is unlikely to account for the large CO_2 deficit in the budget. On the other hand, underestimation of the CO_2 metabolic balance is much more likely, given its large variability and uncertainty around its mean value. Additionally, a systematic underestimation of the CO_2 metabolic rates derived from the diel O_2 method is very possible in Batang Ai given the likely deviation of metabolic quotients around the 1 : 1 line. As an example, when setting the photosynthetic quotient to 1.2 instead of 1, which remains well within the literature range (Lefèvre and Merlivat, 2012; Williams and Robertson, 1991), the average epilimnetic CO_2 mass balance would increase from -17.7 to $4.3\,\mathrm{mmol\,m^{-2}\,d^{-1}}$ in the branches and from -6.5 to $6.2\,\mathrm{mmol\,m^{-2}\,d^{-1}}$ in the main basin, closely matching measured surface fluxes of 4.7 and $7.5\,\mathrm{mmol\,m^{-2}\,d^{-1}}$ in the respective sections. Thus, constraining the metabolic component, especially the $O_2 : CO_2$ quotients, is key for closing the CO_2 epilimnetic budget. Another way to decipher the role of metabolism, given its high uncertainty, is by difference in a mass balance exercise. Assuming mean estimates of all other components are accurate, CO_2 net metabolic rates would have to be equal to -0.8 and $2.1\,\mathrm{mmol\,m^{-2}\,d^{-1}}$ in the branches and main basin respectively for the mass balance to close. This corresponds to a contribution of $-18\,\%$ and $28\,\%$ to the surface CO_2 flux in the respective sections (Fig. 3a and b), suggesting a substantial impact of metabolism on the CO_2 epilimnetic budget.

In the case of CH_4, the measured epilimnetic budget in the branches is surprisingly close to the observed surface flux, largely fuelled by horizontal inputs. Hence, CH_4 emissions from the branches reflect catchment CH_4 loads rather than internal processes. However, in the main basin, these inputs become negligible and the estimated budget does not match measured emissions, indicating a deficit of $0.49\,\mathrm{mmol CH_4\,m^{-2}\,d^{-1}}$. This amount cannot be explained by a potential underestimation of horizontal or vertical inputs since they are two orders of magnitude lower. Similarly, sediment inputs would need to be six time higher than estimated to fulfil the budget deficit, which is unlikely given their much lower range of uncertainty. Thus, the most plausible source to close the mass balance in the main basin would be water column CH_4 production. Although the estimated CH_4 metabolism indicates an average net consumption rather than a net production ($-0.16\,\mathrm{mmol\,m^{-2}\,d^{-1}}$), this mean value is based on only 3 data points and has a high uncertainty associated to it ($\mathrm{SE} = 0.19\,\mathrm{mmol\,m^{-2}\,d^{-1}}$, Table S3). Closing the mass balance would require a net volumetric CH_4 production of about $0.03\,\mathrm{\mu mol\,L^{-1}\,d^{-1}}$ in the water column of the main basin. This value seems plausible since an equal production rate was measured in one of the incubations, and it is at the low end of the range reported in other systems (Bogard et al., 2014; DelSontro et al., 2018b; Donis et al., 2017). This mass balance approach suggests that water column metabolism could be the dominant source of CH_4 in the main basin of Batang Ai, potentially sustaining up to 75 % of surface emissions in that reservoir section (Fig. 3d). Even though this deductive approach is an indirect assessment of water column CH_4 metabolism, it emphasizes its likely key role in the reservoir epilimnetic CH_4 budget, while measured metabolic rates highlight the wide variability of this process and the need for more intensive research into its controls at spatial and temporal scales.

The combination of empirical and mass balance approaches in this study provide not only a partitioning of the contribution of each source/sink in sustaining surface CO_2 and CH_4 fluxes, but also a clear picture of the uncertainties and challenges associated to the estimation of each component.

5 Conclusions

The estimated epilimnetic CO_2 and CH_4 budgets in Batang Ai has helped define the role of different processes in shaping the reservoir surface GHG fluxes to the atmosphere. Results showed that horizontal riverine inputs are important sources of GHG in the reservoir branches (especially for CH_4). This creates a coupling between CO_2 and CH_4 close to the river deltas, which gradually fades along the water flow, until the surface concentrations of the two gases become completely uncoupled in the main basin being driven by different sources. For instance, vertical inputs from the bottom layer contributed significantly to surface CO_2 saturation, while being negligible in the case of CH_4 due to metalimnetic oxidation. Inversely, sediment inputs played a notably greater role in sustaining epilimnetic oversaturation of CH_4 compared to CO_2 in the main basin. Nonetheless, the epilimnetic budgets of both gases presented a high sensitivity to water column metabolism. This result is likely representative of large systems with a high volume of water vs. sediments, which is common for hydroelectric reservoirs. However, metabolic balances of CO_2 and CH_4 were extremely variable in space and time, switching from a net production to a net consumption of the gases, and leading to highly uncertain ecosystem-scale estimates, which emphasizes the key but unconstrained role of metabolism in the overall GHG budgets. Factors driving these metabolic changes are not well defined based on

current knowledge, highlighting the need for further research on the subject. Overall, this study gives an integrative portrait of the relative contribution of different sources to surface CO_2 and CH_4 fluxes in a permanently stratified reservoir including its transition zones (branches). Conclusions and insights derived from this work likely reflect C dynamics in other similar systems and highlight knowledge gaps, guiding future research to better understand and predict aquatic GHG fluxes and regulation.

Data availability. The dataset related to this article is available online through Zenodo at https://doi.org/10.5281/zenodo.4451391 (Soued and Prairie, 2021).

Supplement. The supplement related to this article is available online at: https://doi.org/10.5194/bg-18-1333-2021-supplement.

Author contributions. CS contributed to conceptualization, methodology, validation, formal analysis, investigation, data curation, writing – original draft, writing – review and editing, and project administration. YTP contributed to methodology, validation, investigation, resources, writing – review and editing, supervision, and funding acquisition.

Competing interests. The authors declare that they have no conflict of interest.

Acknowledgements. We are grateful to Karen Lee Suan Ping and Jenny Choo Cheng Yi for their logistic support and participation in sampling campaigns. We also thank Jessica Fong Fung Yee, Amar Ma'aruf Bin Ismawi, Gerald Tawie Anak Thomas, Hilton Bin John, Paula Reis, Sara Mercier-Blais, and Karelle Desrosiers for their help in the field and Katherine Velghe and Marilyne Robidoux for their assistance during laboratory analyses.

Financial support. This research has been supported by the Natural Sciences and Engineering Research Council of Canada (Discovery grant and BES-D) and the Sarawak Energy Berhad.

Review statement. This paper was edited by Sara Vicca and reviewed by three anonymous referees.

References

Adams, D. D.: Diffuse Flux of Greenhouse Gases – Methane and Carbon Dioxide – at the Sediment-Water Interface of Some Lakes and Reservoirs of the World, in: Greenhouse Gas Emissions – Fluxes and Processes, Springer-Verlag, Berlin Heidelberg, 129–153, 2005.

Algesten, G., Sobek, S., Bergström, A. K., Jonsson, A., Tranvik, L. J., and Jansson, M.: Contribution of sediment respiration to summer CO_2 emission from low productive boreal and subarctic lakes, Microb. Ecol., 50, 529–535, https://doi.org/10.1007/s00248-005-5007-x, 2005.

Appling, A. P., Hall, R. O., Arroita, M., and Yackulic, C. B.: StreamMetabolizer: Models for Estimating Aquatic Photosynthesis and Respiration, available at: https://github.com/USGS-R/streamMetabolizer (last access: 1 May 2020), 2018.

Barrette, N. and Laprise, R.: A One-Dimensional Model for Simulating the Vertical Transport of Dissolved CO_2 and CH_4 in Hydroelectric Reservoirs, in: Greenhouse Gas Emissions – Fluxes and Processes, Springer-Verlag, Berlin Heidelberg, 575–595, 2005.

Barros, N., Cole, J. J., Tranvik, L. J., Prairie, Y. T., Bastviken, D., Huszar, V. L. M., del Giorgio, P., and Roland, F.: Carbon emission from hydroelectric reservoirs linked to reservoir age and latitude, Nat. Geosci., 4, 593–596, https://doi.org/10.1038/ngeo1211, 2011.

Bastviken, D., Cole, J. J., Pace, M. L., and Van de-Bogert, M. C.: Fates of methane from different lake habitats: Connecting whole-lake budgets and CH_4 emissions, J. Geophys. Res.-Biogeo., 113, 1–13, https://doi.org/10.1029/2007JG000608, 2008.

Bastviken, D., Tranvik, L. J., Downing, J. A., Crill, P. M., and Enrich-Prast, A.: Freshwater Methane Emissions Offset the Continental Carbon Sink, Science, 331, 50–50, https://doi.org/10.1126/science.1196808, 2011.

Beaulieu, J. J., McManus, M. G., and Nietch, C. T.: Estimates of reservoir methane emissions based on a spatially balanced probabilistic-survey, Limnol. Oceanogr., 61, S27–S40, https://doi.org/10.1002/lno.10284, 2016.

Beaulieu, J. J., DelSontro, T., and Downing, J. A.: Eutrophication will increase methane emissions from lakes and impoundments during the 21st century, Nat. Commun., 10, 3–7, https://doi.org/10.1038/s41467-019-09100-5, 2019.

Berg, A., Lindblad, P., and Svensson, B. H.: Cyanobacteria as a source of hydrogen for methane formation, World J. Microb. Biot., 30, 539–545, https://doi.org/10.1007/s11274-013-1463-5, 2014.

Berggren, M., Lapierre, J.-F., and del Giorgio, P. A.: Magnitude and regulation of bacterioplankton respiratory quotient across freshwater environmental gradients, ISME J., 6, 984–993, https://doi.org/10.1038/ismej.2011.157, 2012.

Bižić, M., Klintzsch, T., Ionescu, D., Hindyieh, M., Guenthel, M., Muro-Pastor, A. M., Eckert, W., Urich, T., Keppler, F., and Grossart, H.-P.: Aquatic and terrestrial Cyanobacteria produce methane, Sci. Adv., 6, eaax5343, https://doi.org/10.1126/sciadv.aax5343, 2019.

Blais, J. M. and Kalff, J.: The influence of lake morphometry on sediment focusing, Limnol. Oceanogr., 40, 582–588, https://doi.org/10.4319/lo.1995.40.3.0582, 1995.

Bogard, M. J. and del Giorgio, P. A.: The role of metabolism in modulating CO_2 fluxes in boreal lakes, Global Biogeochem. Cy., 30, 1509–1525, https://doi.org/10.1002/2016GB005463, 2016.

Bogard, M. J., del Giorgio, P. a, Boutet, L., Chaves, M. C. G., Prairie, Y. T., Merante, A., and Derry, A. M.: Oxic water column methanogenesis as a major component of aquatic CH_4 fluxes., Nat. Commun., 5, 5350, https://doi.org/10.1038/ncomms6350, 2014.

Bogard, M. J., St-Gelais, N. F., Vachon, D., and del Giorgio, P. A.: Patterns of Spring/Summer Open-Water Metabolism Across Boreal Lakes, Ecosystems, 23, 1581–1597, https://doi.org/10.1007/s10021-020-00487-7, 2020.

Borrel, G., Jézéquel, D., Biderre-Petit, C., Morel-Desrosiers, N., Morel, J. P., Peyret, P., Fonty, G., and Lehours, A. C.: Production and consumption of methane in freshwater lake ecosystems, Res. Microbiol., 162, 832–847, https://doi.org/10.1016/j.resmic.2011.06.004, 2011.

Chmiel, H. E., Hofmann, H., Sobek, S., Efremova, T., and Pasche, N.: Where does the river end? Drivers of spatiotemporal variability in CO_2 concentration and flux in the inflow area of a large boreal lake, Limnol. Oceanogr., 65, 1161–1174, https://doi.org/10.1002/lno.11378, 2020.

Coloso, J. J., Cole, J. J., and Pace, M. L.: Difficulty in Discerning Drivers of Lake Ecosystem Metabolism with High-Frequency Data, Ecosystems, 14, 935–948, https://doi.org/10.1007/s10021-011-9455-5, 2011.

Conrad, R.: The global methane cycle: recent advances in understanding the microbial processes involved, Env. Microbiol. Rep., 1, 285–292, https://doi.org/10.1111/j.1758-2229.2009.00038.x, 2009.

Deemer, B. R., Harrison, J. A., Li, S., Beaulieu, J. J., DelSontro, T., Barros, N., Bezerra-Neto, J. F., Powers, S. M., dos Santos, M. A., and Vonk, J. A.: Greenhouse Gas Emissions from Reservoir Water Surfaces: A New Global Synthesis, Bioscience, 66, 949–964, https://doi.org/10.1093/biosci/biw117, 2016.

DelSontro, T., Beaulieu, J. J., and Downing, J. A.: Greenhouse gas emissions from lakes and impoundments: Upscaling in the face of global change, Limnol. Oceanogr. Lett., 3, 64–75, https://doi.org/10.1002/lol2.10073, 2018a.

DelSontro, T., del Giorgio, P. A., and Prairie, Y. T.: No Longer a Paradox: The Interaction Between Physical Transport and Biological Processes Explains the Spatial Distribution of Surface Water Methane Within and Across Lakes, Ecosystems, 21, 1073–1087, https://doi.org/10.1007/s10021-017-0205-1, 2018b.

Donis, D., Flury, S., Stöckli, A., Spangenberg, J. E., Vachon, D., and McGinnis, D. F.: Full-scale evaluation of methane production under oxic conditions in a mesotrophic lake, Nat. Commun., 8, 1–11, https://doi.org/10.1038/s41467-017-01648-4, 2017.

Encinas Fernández, J., Peeters, F., and Hofmann, H.: Importance of the autumn overturn and anoxic conditions in the hypolimnion for the annual methane emissions from a temperate lake, Environ. Sci. Technol., 48, 7297–7304, https://doi.org/10.1021/es4056164, 2014.

Ferland, M. E., Prairie, Y. T., Teodoru, C., and Del Giorgio, P. A.: Linking organic carbon sedimentation, burial efficiency, and long-term accumulation in boreal lakes, J. Geophys. Res.-Biogeo., 119, 836–847, https://doi.org/10.1002/2013JG002345, 2014.

Gebert, J., Köthe, H., and Gröngröft, A.: Prognosis of methane formation by river sediments, J. Soils Sediment., 6, 75–83, https://doi.org/10.1065/jss2006.04.153, 2006.

Gruca-Rokosz, R. and Tomaszek, J. A.: Methane and carbon dioxide in the sediment of a eutrophic reservoir: Production pathways and diffusion fluxes at the sediment-water interface, Water. Air. Soil Poll., 226, https://doi.org/10.1007/s11270-014-2268-3, 2015.

Guérin, F. and Abril, G.: Significance of pelagic aerobic methane oxidation in the methane and carbon budget of a tropical reservoir, J. Geophys. Res.-Biogeo., 112, https://doi.org/10.1029/2006JG000393, 2007.

Guérin, F., Deshmukh, C., Labat, D., Pighini, S., Vongkhamsao, A., Guédant, P., Rode, W., Godon, A., Chanudet, V., Descloux, S., and Serça, D.: Effect of sporadic destratification, seasonal overturn, and artificial mixing on CH_4 emissions from a subtropical hydroelectric reservoir, Biogeosciences, 13, 3647–3663, https://doi.org/10.5194/bg-13-3647-2016, 2016.

Hall, R. O. and Hotchkiss, E. R.: Stream Metabolism, in: Methods in Stream Ecology, Vol. 2, Elsevier, London, UK, 219–233, 2017.

Hanson, P. C., Bade, D. L., Carpenter, S. R., and Kratz, T. K.: Lake metabolism: Relationships with dissolved organic carbon and phosphorus, Limnol. Oceanogr., 48, 1112–1119, https://doi.org/10.4319/lo.2003.48.3.1112, 2003.

Hotchkiss, E. R., Hall Jr, R. O., Sponseller, R. A., Butman, D., Klaminder, J., Laudon, H., Rosvall, M., and Karlsson, J.: Sources of and processes controlling CO_2 emissions change with the size of streams and rivers, Nat. Geosci., 8, 696–699, https://doi.org/10.1038/ngeo2507, 2015.

Huttunen, J. T., Väisänen, T. S., Hellsten, S. K., and Martikainen, P. J.: Methane fluxes at the sediment-water interface in some boreal lakes and reservoirs, Boreal Environ. Res., 11, 27–34, 2006.

Imboden, D. M.: Limnologische Transport- und Nährstoffmodelle, Schweiz. Z. Hydrol., 35, 29–68, https://doi.org/10.1007/BF02502063, 1973.

International Hydropower Association (IHA): GHG measurement guidelines for freshwater reservoirs, The International Hydropower Association, Sutton, London, UK, 2010.

Isidorova, A., Grasset, C., Mendonça, R., and Sobek, S.: Methane formation in tropical reservoirs predicted from sediment age and nitrogen, Sci. Rep.-UK, 9, 1–9, https://doi.org/10.1038/s41598-019-47346-7, 2019.

Kankaala, P., Huotari, J., Tulonen, T., and Ojala, A.: Lake-size dependent physical forcing drives carbon dioxide and methane effluxes from lakes in a boreal landscape, Limnol. Oceanogr., 58, 1915–1930, https://doi.org/10.4319/lo.2013.58.6.1915, 2013.

Karlsson, J., Jansson, M., and Jonsson, A.: Respiration of allochthonous organic carbon in unproductive forest lakes determined by the Keeling plot method, Limnol. Oceanogr., 52, 603–608, https://doi.org/10.4319/lo.2007.52.2.0603, 2007.

Kim, B., Choi, K., Kim, C., Lee, U. H., and Kim, Y. H.: Effects of the summer monsoon on the distribution and loading of organic carbon in a deep reservoir, Lake Soyang, Korea, Water Resour., 34, 3495–3504, https://doi.org/10.1016/S0043-1354(00)00104-4, 2000.

Kimmel, B. L. and Groeger, A. W.: Factors Controlling Primary Production in Lakes and Reservoirs: a Perspective, Lake Reserv. Manag., 1, 277–281, https://doi.org/10.1080/07438148409354524, 1984.

Kindler, R., Siemens, J., Kaiser, K., Walmsley, D. C., Bernhofer, C., Buchmann, N., Cellier, P., Eugster, W., Gleixner, G., Grunwald, T., Heim, A., Ibrom, A., Jones, S. K., Jones, M., Klumpp, K., Kutsch, W., Larsen, K. S., Lehuger, S., Loubet, B., Mckenzie, R., Moors, E., Osborne, B., Pilegaard, K., Rebmann, C., Saunders, M., Schmidt, M. W. I., Schrumpf, M., Seyfferth, J., Skiba, U., Soussana, J. F., Sutton, M. A., Tefs, C.,

Vowinckel, B., Zeeman, M. J., and Kaupenjohann, M.: Dissolved carbon leaching from soil is a crucial component of the net ecosystem carbon balance, Glob. Change Biol., 17, 1167–1185, https://doi.org/10.1111/j.1365-2486.2010.02282.x, 2011.

Kreling, J., Bravidor, J., McGinnis, D. F., Koschorreck, M., and Lorke, A.: Physical controls of oxygen fluxes at pelagic and benthic oxyclines in a lake, Limnol. Oceanogr., 59, 1637–1650, https://doi.org/10.4319/lo.2014.59.5.1637, 2014.

Lefèvre, N. and Merlivat, L.: Carbon and oxygen net community production in the eastern tropical Atlantic estimated from a moored buoy, Global Biogeochem. Cy., 26, https://doi.org/10.1029/2010GB004018, 2012.

Lenhart, K., Klintzsch, T., Langer, G., Nehrke, G., Bunge, M., Schnell, S., and Keppler, F.: Evidence for methane production by the marine algae *Emiliania huxleyi*, Biogeosciences, 13, 3163–3174, https://doi.org/10.5194/bg-13-3163-2016, 2016.

Lewis, W. M.: Biogeochemistry of tropical lakes, SIL Proceedings, 1922–2010 Internationale Vereinigung für Theoretische und Angewandte Limnologie: Verhandlungen, 30, 1595–1603, https://doi.org/10.1080/03680770.2009.11902383, 2010.

Li, M., Peng, C., Wang, M., Xue, W., Zhang, K., Wang, K., Shi, G., and Zhu, Q.: The carbon flux of global rivers: A re-evaluation of amount and spatial patterns, Ecol. Indic., 80, 40–51, https://doi.org/10.1016/j.ecolind.2017.04.049, 2017.

Loken, L. C., Crawford, J. T., Schramm, P. J., Stadler, P., Desai, A. R., and Stanley, E. H.: Large Spatial and Temporal Variability of Carbon Dioxide and Methane in a Eutrophic Lake, J. Geophys. Res.-Biogeo., 124, 2248–2266, https://doi.org/10.1029/2019JG005186, 2019.

Lupon, A., Denfeld, B. A., Laudon, H., Leach, J., Karlsson, J., and Sponseller, R. A.: Groundwater inflows control patterns and sources of greenhouse gas emissions from streams, Limnol. Oceanogr., 64, 1545–1557, https://doi.org/10.1002/lno.11134, 2019.

Maavara, T., Lauerwald, R., Regnier, P., and Van Cappellen, P.: Global perturbation of organic carbon cycling by river damming, Nat. Commun., 8, 1–10, https://doi.org/10.1038/ncomms15347, 2017.

Martinsen, K. T., Kragh, T., and Sand-Jensen, K.: Carbon dioxide efflux and ecosystem metabolism of small forest lakes, Aquat. Sci., 82, 9, https://doi.org/10.1007/s00027-019-0682-8, 2020.

Monteith, D. T., Stoddard, J. L., Evans, C. D., De Wit, H. A., Forsius, M., Høgåsen, T., Wilander, A., Skjelkvåle, B. L., Jeffries, D. S., Vuorenmaa, J., Keller, B., Kopécek, J., and Vesely, J.: Dissolved organic carbon trends resulting from changes in atmospheric deposition chemistry, Nature, 450, 537–540, https://doi.org/10.1038/nature06316, 2007.

Natchimuthu, S., Sundgren, I., Gålfalk, M., Klemedtsson, L., and Bastviken, D.: Spatiotemporal variability of lake pCO2 and CO_2 fluxes in a hemiboreal catchment, J. Geophys. Res.-Biogeo., 122, 30–49, https://doi.org/10.1002/2016JG003449, 2017.

Oakey, N. S.: Determination of the Rate of Dissipation of Turbulent Energy from Simultaneous Temperature and Velocity Shear Microstructure Measurements, J. Phys. Oceanogr., 12, 256–271, https://doi.org/10.1175/1520-0485(1982)012<0256:DOTROD>2.0.CO;2, 1982.

Odum, H. T.: Primary Production in Flowing Waters1, Limnol. Oceanogr., 1, 102–117, https://doi.org/10.4319/lo.1956.1.2.0102, 1956.

Osborn, T. R.: Estimates of the Local Rate of Vertical Diffusion from Dissipation Measurements, J. Phys. Oceanogr., 10, 83–89, https://doi.org/10.1175/1520-0485(1980)010<0083:EOTLRO>2.0.CO;2, 1980.

Pace, M. L. and Prairie, Y. T.: Respiration in lakes, in Respiration in Aquatic Ecosystems, Oxford University Press, Oxford, UK, 103–121, 2005.

Pacheco, F. S., Soares, M. C. S., Assireu, A. T., Curtarelli, M. P., Roland, F., Abril, G., Stech, J. L., Alvalá, P. C., and Ometto, J. P.: The effects of river inflow and retention time on the spatial heterogeneity of chlorophyll and water–air CO_2 fluxes in a tropical hydropower reservoir, Biogeosciences, 12, 147–162, https://doi.org/10.5194/bg-12-147-2015, 2015.

Paranaíba, J. R., Barros, N., Mendonça, R., Linkhorst, A., Isidorova, A., Roland, F., Almeida, R. M., and Sobek, S.: Spatially Resolved Measurements of CO_2 and CH_4 Concentration and Gas-Exchange Velocity Highly Influence Carbon-Emission Estimates of Reservoirs, Environ. Sci. Technol., 52, 607–615, https://doi.org/10.1021/acs.est.7b05138, 2018.

Pasche, N., Hofmann, H., Bouffard, D., Schubert, C. J., Lozovik, P. A., and Sobek, S.: Implications of river intrusion and convective mixing on the spatial and temporal variability of under-ice CO_2, Inland Waters, 9, 162–176, https://doi.org/10.1080/20442041.2019.1568073, 2019.

Pebesma, E. J.: Multivariable geostatistics in S: the gstat package, Comput. Geosci., 30, 683–691, https://doi.org/10.1016/j.cageo.2004.03.012, 2004.

Prairie, Y. T., Duarte, C. M., and Kalff, J.: Unifying Nutrient–Chlorophyll Relationships in Lakes, Can. J. Fish. Aquat. Sci., 46, 1176–1182, https://doi.org/10.1139/f89-153, 1989.

Prairie, Y. T., Bird, D. F., and Cole, J. J.: The summer metabolic balance in the epilimnion of southeastern Quebec lakes, Limnol. Oceanogr., 47, 316–321, https://doi.org/10.4319/lo.2002.47.1.0316, 2002.

Prairie, Y. T., Alm, J., Beaulieu, J., Barros, N., Battin, T., Cole, J., del Giorgio, P., DelSontro, T., Guérin, F., Harby, A., Harrison, J., Mercier-Blais, S., Serça, D., Sobek, S., and Vachon, D.: Greenhouse Gas Emissions from Freshwater Reservoirs: What Does the Atmosphere See?, Ecosystems, 21, 1058–1071, https://doi.org/10.1007/s10021-017-0198-9, 2018.

Pu, J., Li, J., Zhang, T., Martin, J. B., and Yuan, D.: Varying thermal structure controls the dynamics of CO_2 emissions from a subtropical reservoir, south China, Water Resour., 178, 115831, https://doi.org/10.1016/j.watres.2020.115831, 2020.

R Core Team: R: A language and environment for statistical computing, available at: https://www.r-project.org/, 2017.

Rasilo, T., Hutchins, R. H. S., Ruiz-González, C., and del Giorgio, P. A.: Transport and transformation of soil-derived CO_2, CH_4 and DOC sustain CO_2 supersaturation in small boreal streams, Sci. Total Environ., 579, 902–912, https://doi.org/10.1016/j.scitotenv.2016.10.187, 2017.

Raymond, P. A., Hartmann, J., Lauerwald, R., Sobek, S., McDonald, C., Hoover, M., Butman, D., Striegl, R., Mayorga, E., Humborg, C., Kortelainen, P., Dürr, H., Meybeck, M., Ciais, P., and Guth, P.: Global carbon dioxide emissions from inland waters, Nature, 503, 355–359, https://doi.org/10.1038/nature12760, 2013.

Reis, P. C. J., Thottathil, S. D., Ruiz-González, C., and Prairie, Y. T.: Niche separation within aerobic methanotrophic bacteria across

lakes and its link to methane oxidation rates, Environ. Microbiol., 22, 738–751, https://doi.org/10.1111/1462-2920.14877, 2020.

Roland, F., Vidal, L. O., Pacheco, F. S., Barros, N. O., Assireu, A., Ometto, J. P. H. B., Cimbleris, A. C. P., and Cole, J. J.: Variability of carbon dioxide flux from tropical (Cerrado) hydroelectric reservoirs, Aquat. Sci., 72, 283–293, https://doi.org/10.1007/s00027-010-0140-0, 2010.

Rudorff, C. M., Melack, J. M., MacIntyre, S., Barbosa, C. C. F., and Novo, E. M. L. M.: Seasonal and spatial variability of CO_2 emission from a large floodplain lake in the lower Amazon, J. Geophys. Res.-Biogeo., 116, 1–12, https://doi.org/10.1029/2011JG001699, 2011.

Sand-Jensen, K. and Staehr, P. A.: Net heterotrophy in small danish lakes: A widespread feature over gradients in trophic status and land cover, Ecosystems, 12, 336–348, https://doi.org/10.1007/s10021-008-9226-0, 2009.

Sarawak Government: The Geography of Sarawak, available at: https://www.sarawak.gov.my/web/home/article_view/159/176/ (last access: 3 May 2019), 2019.

Schmid, M., De Batist, M., Granin, N. G., Kapitanov, V. A., McGinnis, D. F., Mizandrontsev, I. B., Obzhirov, A. I., and Wüest, A.: Sources and sinks of methane in Lake Baikal: A synthesis of measurements and modeling, Limnol. Oceanogr., 52, 1824–1837, https://doi.org/10.4319/lo.2007.52.5.1824, 2007.

Solomon, C. T., Bruesewitz, D. A., Richardson, D. C., Rose, K. C., Van de Bogert, M. C., Hanson, P. C., Kratz, T. K., Larget, B., Adrian, R., Leroux Babin, B., Chiu, C. Y., Hamilton, D. P., Gaiser, E. E., Hendricks, S., Istvá, V., Laas, A., O'Donnell, D. M., Pace, M. L., Ryder, E., Staehr, P. A., Torgersen, T., Vanni, M. J., Weathers, K. C., and Zhu, G.: Ecosystem respiration: Drivers of daily variability and background respiration in lakes around the globe, Limnol. Oceanogr., 58, 849–866, https://doi.org/10.4319/lo.2013.58.3.0849, 2013.

Soued, C. and Prairie, Y. T.: The carbon footprint of a Malaysian tropical reservoir: measured versus modelled estimates highlight the underestimated key role of downstream processes, Biogeosciences, 17, 515–527, https://doi.org/10.5194/bg-17-515-2020, 2020.

Soued, C. and Prairie, Y.: Carbon dioxide, methane, and chemical data from Batang Ai reservoir (Version 1.1.0), Zenodo, https://doi.org/10.5281/zenodo.4451391, 2021.

St. Louis, V. L., Kelly, C. A., Duchemin, É., Rudd, J. W. M., and Rosenberg, D. M.: Reservoir Surfaces as Sources of Greenhouse Gases to the Atmosphere: A Global Estimate, Bioscience, 50, 766–775, https://doi.org/10.1641/0006-3568(2000)050[0766:RSASOG]2.0.CO;2, 2000.

Staehr, P. A. and Sand-Jensen, K.: Temporal dynamics and regulation of lake metabolism, Limnol. Oceanogr., 52, 108–120, https://doi.org/10.4319/lo.2007.52.1.0108, 2007.

Tan, A. C.: Water and sediment quality of Batang Ai Reservoir, available at: https://ir.unimas.my/id/eprint/10428/ (last access: 21 April 2020), 2015.

Tang, K. W., McGinnis, D. F., Frindte, K., Brüchert, V., and Grossart, H. P.: Paradox reconsidered: Methane oversaturation in well-oxygenated lake waters, Limnol. Oceanogr., 59, 275–284, https://doi.org/10.4319/lo.2014.59.1.0275, 2014.

Tank, J. L., Rosi-Marshall, E. J., Griffiths, N. A., Entrekin, S. A., and Stephen, M. L.: A review of allochthonous organic matter dynamics and metabolism in streams, J. N. Am. Benthol. Soc., 29, 118–146, https://doi.org/10.1899/08-170.1, 2010.

Teodoru, C. R., Prairie, Y. T., and del Giorgio, P. A.: Spatial Heterogeneity of Surface CO_2 Fluxes in a Newly Created Eastmain-1 Reservoir in Northern Quebec, Canada, Ecosystems, 14, 28–46, https://doi.org/10.1007/s10021-010-9393-7, 2011.

Thornton, K. W., Kimmel, B. L., and Payne, F. E.: Reservoir Limnology: Ecological Perspectives, John Wiley and Sons, Inc., New York, 1990.

Thottathil, S. D., Reis, P. C. J., del Giorgio, P. A., and Prairie, Y. T.: The Extent and Regulation of Summer Methane Oxidation in Northern Lakes, J. Geophys. Res.-Biogeo., 123, 3216–3230, https://doi.org/10.1029/2018JG004464, 2018.

Thottathil, S. D., Reis, P. C. J., and Prairie, Y. T.: Methane oxidation kinetics in northern freshwater lakes, Biogeochemistry, 143, 105–116, https://doi.org/10.1007/s10533-019-00552-x, 2019.

Tranvik, L. J., Cole, J. J., and Prairie, Y. T.: The study of carbon in inland waters-from isolated ecosystems to players in the global carbon cycle, Limnol. Oceanogr. Lett., 3, 41–48, https://doi.org/10.1002/lol2.10068, 2018.

Vachon, D. and del Giorgio, P. A.: Whole-Lake CO_2 Dynamics in Response to Storm Events in Two Morphologically Different Lakes, Ecosystems, 17, 1338–1353, https://doi.org/10.1007/s10021-014-9799-8, 2014.

Vachon, D., Langenegger, T., Donis, D., and McGinnis, D. F.: Influence of water column stratification and mixing patterns on the fate of methane produced in deep sediments of a small eutrophic lake, Limnol. Oceanogr., 64, 2114–2128, https://doi.org/10.1002/lno.11172, 2019.

Vachon, D., Sadro, S., Bogard, M. J., Lapierre, J., Baulch, H. M., Rusak, J. A., Denfeld, B. A., Laas, A., Klaus, M., Karlsson, J., Weyhenmeyer, G. A. and Giorgio, P. A.: Paired O_2–CO 2 measurements provide emergent insights into aquatic ecosystem function, Limnol. Oceanogr. Lett., 5, 287–294, https://doi.org/10.1002/lol2.10135, 2020.

Venkiteswaran, J. J., Schiff, S. L., St. Louis, V. L., Matthews, C. J. D., Boudreau, N. M., Joyce, E. M., Beaty, K. G., and Bodaly, R. A.: Processes affecting greenhouse gas production in experimental boreal reservoirs, Global Biogeochem. Cy., 27, 567–577, https://doi.org/10.1002/gbc.20046, 2013.

Wang, Q., Dore, J. E., and McDermott, T. R.: Methylphosphonate metabolism by Pseudomonas sp. populations contributes to the methane oversaturation paradox in an oxic freshwater lake, Environ. Microbiol., 19, 2366–2378, https://doi.org/10.1111/1462-2920.13747, 2017.

Wilkinson, G. M., Buelo, C. D., Cole, J. J., and Pace, M. L.: Exogenously produced CO_2 doubles the CO_2 efflux from three north temperate lakes, Geophys. Res. Lett., 43, 1996–2003, https://doi.org/10.1002/2016GL067732, 2016.

Williams, P. J. I. and Robertson, J. E.: Overall planktonic oxygen and carbon dioxide metabolisms: the problem of reconciling observations and calculations of photosynthetic quotients, J. Plankton Res., 13, 153–169, https://doi.org/10.1093/oxfordjournals.plankt.a042366, 1991.

Winslow, L., Read, J., Woolway, R., Brentrup, J., Leach, T., Zwart, J., Albers, S., and Collinge, D.: rLakeAnalyzer: Lake Physics Tools, available at: https://cran.r-project.org/package=rLakeAnalyzer, last access: 4 December 2018.

Wüest, A. and Lorke, A.: Small-Scale Turbulence and Mixing: Energy Fluxes in Stratified Lakes, in: Encyclopedia of Inland Waters, Elsevier, 628–635, 2009.

Zarfl, C., Lumsdon, A. E., Berlekamp, J., Tydecks, L., and Tockner, K.: A global boom in hydropower dam construction, Aquat. Sci., 77, 161–170, https://doi.org/10.1007/s00027-014-0377-0, 2015.

Zhang, Q., Tao, Z., Ma, Z., Gao, Q., Deng, H., Xu, P., Ding, J., Wang, Z., and Lin, Y.: Hydro-ecological controls on riverine organic carbon dynamics in the tropical monsoon region, Sci. Rep.-UK, 9, 1–11, https://doi.org/10.1038/s41598-019-48208-y, 2019.